JACS
JOURNAL OF THE AMERICAN CHEMICAL SOCIETY
Communication
pubs.acs.org/JACS

Tunable Narrow Band Emissions from Dye-Sensitized Core/Shell/Shell Nanocrystals in the Second Near-Infrared Biological Window

Wei Shao,[‡,†] Guanying Chen,[*,‡,†] Andrey Kuzmin,[†] Hilliard L. Kutscher,[†] Artem Pliss,[†] Tymish Y. Ohulchanskyy,[†,§] and Paras N. Prasad[*,†]

[†]Institute for Lasers, Photonics, and Biophotonics and Department of Chemistry, University at Buffalo, State University of New York, Buffalo, New York 14260, United States

[‡]School of Chemistry and Chemical Engineering, Harbin Institute of Technology, Harbin, Heilongjiang 150001, People's Republic of China

[§]College of Optoelectronic Engineering, Shenzhen University, Shenzhen, Guangdong 518060, People's Republic of China

Supporting Information

ABSTRACT: We introduce a hybrid organic−inorganic system consisting of epitaxial $NaYF_4$:Yb^{3+}/X^{3+}@$NaYbF_4$@$NaYF_4$:Nd^{3+} (X = null, Er, Ho, Tm, or Pr) core/shell/shell (CSS) nanocrystal with organic dye, indocyanine green (ICG) on the nanocrystal surface. This system is able to produce a set of narrow band emissions with a large Stokes-shift (>200 nm) in the second biological window of optical transparency (NIR-II, 1000−1700 nm), by directional energy transfer from light-harvesting surface ICG, via lanthanide ions in the shells, to the emitter X^{3+} in the core. Surface ICG not only increases the NIR-II emission intensity of inorganic CSS nanocrystals by ∼4-fold but also provides a broadly excitable spectral range (700−860 nm) that facilitates their use in bioapplications. We show that the NIR-II emission from ICG-sensitized Er^{3+}-doped CSS nanocrystals allows clear observation of a sharp image through 9 mm thick chicken breast tissue, and emission signal detection through 22 mm thick tissue yielding a better imaging profile than from typically used Yb/Tm-codoped upconverting nanocrystals imaged in the NIR-I region (700−950 nm). Our result on in vivo imaging suggests that these ICG-sensitized CSS nanocrystals are suitable for deep optical imaging in the NIR-II region.

Optical imaging is an important tool in early detection and diagnosis of disease, as it enables noninvasive real-time feedback using nonharmful nonionizing radiation, provides high spatial resolution, and examines structures across a wide range of size and type.[1−4] Despite these merits, this technique suffers from limited imaging depth (1−2 mm, for fluorophores emitting in the visible region of 400−700 nm) and autofluorescence background,[4] restricting the ability to unravel biological complexities in deep tissue. Traditional near-infrared light (NIR-I, 700−950 nm), deemed the first biological window, penetrates deeper than visible range light, due to reduced light absorption and scattering.[5] Yet, in practice, this NIR-I window is not optimal because tissue autofluorescence still produces substantial background noise, and the existence of photon scattering limits the tissue penetration depth.[6] Photon scattering scales as $\lambda^{-\alpha}$, where λ is the wavelength and α = 0.2−4 for biological tissues.[7] Recent experimental and simulation results show that optical imaging in the longer wavelength NIR-II region (1000−1700 nm), also referred to as the second biological window,[8,9] significantly improves the signal-to-noise ratio, probes tissue at centimeter range of depth, and achieves micrometer-scale resolution at depths of millimeters, which is not possible with fluorescence imaging in the NIR-I window.[8−15] However, limited success has been made in the development of photoluminescent contrast agent in the NIR-II region. To date, only a few reports exist on the use of carbon nanotubes,[6,11−13] Ag_2S quantum dots,[14,15] and small organic molecules (CH1055),[8] but these materials are limited in terms of their broad-band emission, lack of tunable emission, short-lifetime, and low emission quantum yields.

Lanthanide-doped nanoparticles exhibit low toxicity, narrow band emission, long emission lifetime, nonphotobleaching and nonblinking, making them promising for biological imaging.[1] However, most existing reports are only exploiting upconversion (anti-Stokes emission) of light, typically at ∼980 nm, into shorter NIR-I (∼800 nm) or visible region (anti-Stokes emission) for in vitro and in vivo bioimaging.[10,16,17] NIR-II photoluminescence bioimaging from lanthanide-doped nanoparticles was reported utilizing Yb^{3+} ion as the sensitizer.[18−20] However, the excitation is limited to ∼980 nm that induces deleterious heating effects due to the strong absorption by water molecules, causing serious damage to cells and biological tissues.[21] Our group as well as others have recently shown that the Nd^{3+} ion is not only able to emit NIR-II emission (∼1050 and ∼1300 nm)[22] but also efficiently sensitize Yb^{3+} ions when excited at a biocompatible wavelength of ∼800 nm where absorption by water is minimal.[23−25] However, multicolor NIR-II emission from lanthanide ions with ∼800 nm excitation and beyond remains elusive. Moreover, lanthanide-doped nanoparticles typically possess narrow (∼10 nm) and weak absorption (cross section of 10^{-20} cm^{-2}, 1000-fold lower than an organic dye) due to the nature of 4f−4f transition of lanthanide ion, limiting their brightness and excitation spectral range.[26]

Here, we report a hybrid organic−inorganic system consisting of an epitaxial $NaYF_4$:Yb^{3+}/X^{3+}@$NaYbF_4$@$NaYF_4$:Nd^{3+} (X =

Received: August 30, 2016
Published: December 1, 2016

DOI: 10.1021/jacs.6b08973
J. Am. Chem. Soc. 2016, 138, 16192−16195

null, Er, Ho, Tm, or Pr) core/shell/shell (CSS) nanocrystal with organic NIR dyes (indocyanine green, ICG) attached to the CSS nanocrystal surface. This hybrid system is able to produce efficient multicolor narrow-band NIR-II emissions with excitation across a broad spectral range (Figure 1b), allowing

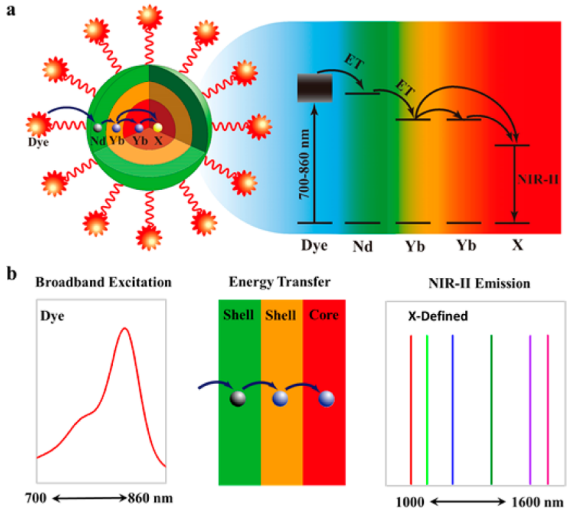

Figure 1. Schematic illustrations of (a) energy transfer pathway from ICG on the surface of $NaYF_4$:Yb^{3+}/X^{3+}@$NaYbF_4$@$NaYF_4$:Nd^{3+} nanocrystal, to the Nd^{3+} ions in the outer shell, then to the Yb^{3+} in the inner shell, and finally to the Yb^{3+}/X^{3+} (X = null, Er, Ho, Tm, or Pr) in the core, producing large Stokes-shifted NIR-II emissions; (b) the functional roles of ICG (providing excitation between 700 and 860 nm, absorption spectrum for 40 μg/mL in DMF), the core/shell/shell structure (spatial isolation of the core from surrounding quenching center, and directing energy transfer to the core), and the activator of varying type (entailing defined narrow band emission in the NIR-II range).

imaging through thick biological tissues. The structure of ICG-sensitized CSS nanocrystal is depicted in Figure 1a, whereby ICG (absorption cross section of 10^{-16} cm^{-2}) can harvest NIR light in a broad range, entailing a wide excitation spectral range (700–860 nm).[27] The harvested energy is then nonradiatively transferred to the Nd^{3+} ions in the outer shell layer, then to the Yb^{3+} ions in the inner shell layer, and finally to the Yb^{3+}/X^{3+} ion pair (X = null, Er, Ho, Tm, or Pr) in the inorganic core to entail a plethora of emitter-defined narrow emissions in the NIR-II range (Figure 1a). The CSS structure employed here not only suppresses surface-related quenching of the core nanocrystal by spatial isolation from the environment but also elicits directional energy flow all the way to the core nanocrystal to emit large Stoke-shifted NIR-II emission.

Hexagonal $NaYF_4$ with low phonon energy is chosen as the inorganic host material to build the CSS structure because it is known to be one of the most efficient materials for lanthanide emission.[1] CSS nanocrystals of $NaYF_4$:30%Yb^{3+}/2%X^{3+}@$NaYbF_4$@$NaYF_4$:30%Nd^{3+} (X = null, Er, Ho, Tm, or Pr) were synthesized following an adapted procedure from the literature.[28] Transmission electron microscopy (TEM) results (Figure 2a) show that the $NaYF_4$:Yb^{3+}/X^{3+} core, the $NaYF_4$:Yb^{3+}/X^{3+}@$NaYbF_4$ core/shell, and the $NaYF_4$:Yb^{3+}/X^{3+}@$NaYbF_4$@$NaYF_4$:Nd^{3+} CSS nanocrystals are spherical and uniform, with a mean size of 32, 43, and 52 nm, respectively (Figure S1). This suggests that each shell layer has a thickness of ~5 nm for the CSS nanocrystals. X-ray diffraction (XRD) results indicate that the core, the core/shell, and the CSS nanocrystals

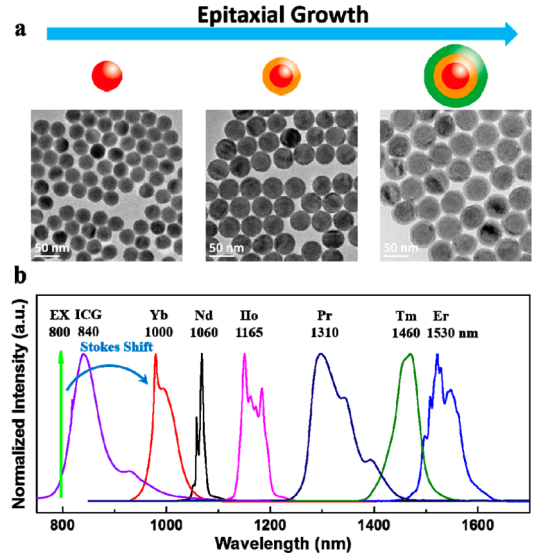

Figure 2. (a) TEM images of $NaYF_4$:Yb^{3+}/Er^{3+} core, $NaYF_4$:Yb,Er@$NaYbF_4$ core/shell, $NaYF_4$:Yb^{3+}/Er^{3+}@$NaYbF_4$@$NaYF_4$:Nd^{3+} core/shell/shell nanocrystals (from left to right). (b) Normalized multiband NIR-II emission peaks from nanocrystals of $NaYF_4$:Yb^{3+}/X^{3+}@$NaYbF_4$@$NaYF_4$:Nd^{3+} (X = null, Er, Ho, Tm, or Pr) dispersed in hexane (1 wt %). The emission peak at 1060 nm from hexane-dispersed $NaYF_4$:Nd^{3+} nanocrystals is added as a separate NIR-II emission band. Excitation at 800 nm with a power density of 4 W/cm^2.

are of hexagonal crystallographic phase with good crystallinity (Figure S3). When excited at ~800 nm, the CSS nanocrystals of $NaYF_4$:30%Yb^{3+},2%X^{3+}@$NaYbF_4$@$NaYF_4$:30%Nd^{3+} (X = null, Er, Ho, Tm, or Pr) are able to emit multiple narrow band emissions with a large Stokes shift (>200 nm) at 1000 nm for Yb^{3+} (X = null), 1165 nm (X = Ho), 1310 nm (X = Pr), 1460 nm (X = Tm), and 1530 nm (X = Er) (Figure 2b and Figure S4), respectively.[29] The emission at 1060 nm of Nd^{3+} from $NaYF_4$:Nd^{3+} nanocrystals is included in Figure 2b as a reference. These narrow emission peaks cover the whole spectral range between 1000 and 1600 nm, implying their suitability for multiplexed bioimaging in the NIR-II region. Note that the existence of the $NaYbF_4$ layer in the CSS structure is important to maximize emission from the emitter X, as this layer can suppress detrimental cross-relaxation processes between X and Nd^{3+} by spatial isolation, and enhance energy transfer from the outer shell to the core by introducing Yb-mediated energy migration (Figure S5).

We then investigated the sensitization effect of ICG on the CSS nanocrystal to impart a broad excitation spectral range and enhance the brightness, aiming to facilitate the use of these nanoparticles in optical imaging. We selected ICG because of its high NIR luminescence efficiency and the strong overlapping of its emission spectrum with the absorption spectrum of Nd ions. The long-chain ligand of oleic acid (OA) used during synthesis of CSS nanocrystals was first replaced by a short ionic ligand of nitrosonium tetrafluoroborate ($NOBF_4$) (no luminescence quenching was observed, Figure S6), followed by mixing with ICG to enable attachment to the nanocrystal surface through the tetrafluoroborate group (Figure S7).[26] The introduction of ICG into the CSS nanocrystal dispersion is able to enhance the emission intensities of CSS nanocrystals, independent of the doped emitter (X) type. The dependency of the integrated emission intensity from CSS nanocrystals doped with emitter of Er^{3+} (1530 nm), Ho^{3+} (1165 nm), and Tm^{3+} (1460 nm) on ICG

DOI: 10.1021/jacs.6b08973
J. Am. Chem. Soc. 2016, 138, 16192–16195

concentration are shown in Figure 3a. The optimized ICG concentration was revealed to be ~40−45 μg/mL, which

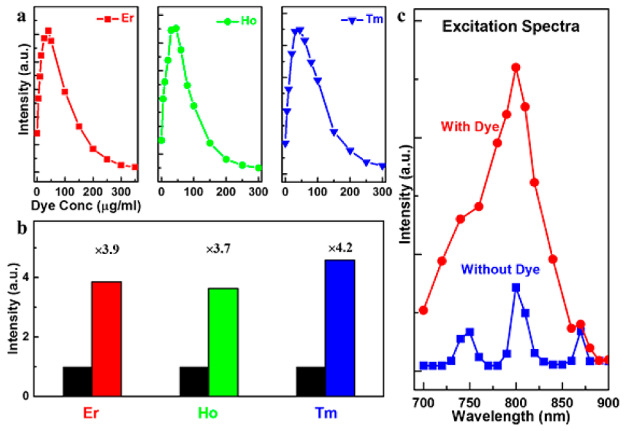

Figure 3. (a) Dependence of the integrated emission intensities from the $^4I_{13/2}$ level of Er^{3+} (1530 nm), from the $^5I_6$ level of Ho^{3+} (1165 nm), and from the $^4H_4$ level of Tm^{3+} (1460 nm) of ICG-sensitized CSS nanocrystals versus the ICG concentration. (b) Histogram shows the comparison of integrated emission intensities from Er^{3+}-, Ho^{3+}-, or Tm^{3+}-doped CSS nanoparticles with and without ($NOBF_4$-capped) ICG sensitization (the intensities without dye sensitization were normalized for clarification). (c) Photoluminescent excitation spectra (for the integrated emission intensity from the $^4I_{13/2}$ state of Er^{3+}) for Er^{3+}-doped CSS nanocrystals with and without ($NOBF_4$-capped) ICG sensitization.

resulted in 3.9-, 3.7-, and 4.2-fold enhancement for the $NaYF_4$:30%Yb^{3+}/2%X^{3+}@$NaYbF_4$@$NaYF_4$:30%Nd^{3+} CSS nanocrystals doped with X = Er^{3+}, Ho^{3+}, and Tm^{3+}, respectively (Figures 3b and S9). The efficiency of energy transfer from ICG to the nanoparticle was determined to be ~75% (Figure S11); while the luminescence quantum yield of ICG sensitized Er^{3+}-doped CSS nanoparticles was measured to be ~13% (Figure S10). The dependence of emission intensity on ICG concentration is possibly a result of the competition between the ICG dye antenna effect (enhancing light harvesting, Figure S8) and the dye−dye quenching interaction (deactivation of harvested energy) on the surface of the CSS nanocrystals. The 4-fold excitation intensity difference at 800 nm (Figure 3c) is in good agreement with 4-fold emission enhancement induced by ICG sensitization in Figure 3b. Moreover, the broad-band excitation peak from ICG-attached CSS nanocrystals is in marked contrast to the sharp and narrow band peak from pure CSS nanocrystal, providing a direct evidence of ICG sensitization. The significantly widened excitation spectrum permits these ICG-sensitized CSS to be excited within a broad spectral range from 700 to 870 nm, facilitating their applications with multiple different light sources.

The enhancement of emission intensity caused by the ICG sensitization effect can also be clearly seen by comparing the NIR-II photoluminescent image of ICG-sensitized CSS nanocrystals versus pure CSS nanocrystals (dispersed in DMF) using a NIR-sensitive InGaAs camera (New Imaging Technologies) (Figure 4a). To test whether ICG-sensitized CSS nanocrystals are suitable for deep tissue optical bioimaging, we imaged the NIR-II luminescence of polymer pattern (the letter "A", 3 × 3 cm) incorporating ICG-sensitized $NaYF_4$:30%Yb^{3+}/2%Er^{3+}@$NaYbF_4$@$NaYF_4$:30% Nd^{3+} nanocrystals through tissue (chicken breast) of known thickness (Figure S12). The polymer pattern was made by mixing the ICG-sensitized CSS nanocrystals

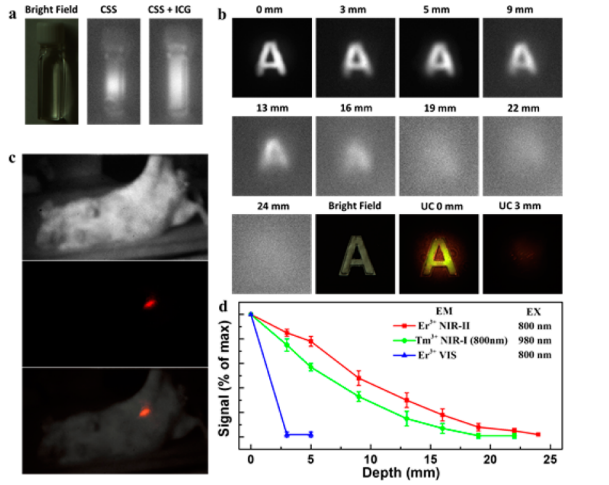

Figure 4. (a) NIR-II photoluminescent imaging of Er^{3+}-doped CSS ($NaYF_4$:30%Yb^{3+},2%Er@$NaYbF_4$@$NaYF_4$:30%Nd) nanocrystals with and without ICG sensitization (excited at 800 nm). (b) NIR-II photoluminescent image of the polymer pattern containing ICG-sensitized Er^{3+}-doped CSS nanocrystals through chicken breast tissue of varied thickness (excited at 800 nm). (c) NIR-II photoluminescent bioimaging of a mouse with subcutaneous injection (excited at 800 nm). (d) Detected intensity of NIR-II emission from ICG-sensitized Er^{3+}-doped CSS nanocrystals (excited at 800 nm), green upconversion emission (at ~540 nm) from the same nanocrystal (excited at 800 nm), as well as NIR-I upconversion emission (800 nm) from $NaYF_4$:30% Yb^{3+}/0.5%Tm^{3+}@$NaYF_4$ core/shell nanocrystals (excited at 980 nm), versus the imaging depth. The excitation density at both 800 and 980 nm is ~0.2 W/cm^2.

with polystyrene beads in chloroform to yield a transparent and uniform gel, followed by casting through a homemade mold with natural evaporation of the solvent. The green upconversion emission of Er^{3+} (~540 nm) from the same pattern was utilized as a control study (taken by a visible-sensitive camera), which previously was employed for upconversion bioimaging (Figure 4b).[21] The sharp image of the polymer pattern can be visualized by NIR-II emission with a tissue depth of up to 9 mm, and the emission signal can be detected even with a depth of up to 23 mm. However, both the letter image and the emission signal are hard to be detected when using green upconversion through a tissue thickness of merely 3 mm under the same excitation at 800 nm (Figure 4b,d). This result clearly implies the appropriateness of NIR-II emission from ICG-sensitized CSS nanocrystals for deep tissue optical imaging. Moreover, it has been established that Yb^{3+}/Tm^{3+}-codoped upconversion nanocrystals are good for deep optical bioimaging, as both the excitation of ~980 nm and the upconverted emission at ~800 nm fall within the first biological window (NIR-I region).[5] Next, we utilized the upconversion emission from typically used $NaYF_4$:30%Yb^{3+}/0.5%Tm^{3+}@$NaYF_4$ core/shell nanocrystals as a positive control to probe the deep tissue imaging ability of NIR-II emission from ICG-sensitized Er doped CSS nanocrystals (Figure 4d). It was found that the NIR-II emission is better than upconverted emission at 800 nm for deep tissue optical imaging, by showing improved signal at all defined tissue depths, possibly owing to reduced photon scattering in the NIR-II window than in the NIR-I window. This conclusion was supported by the observation of a blurred upconversion image (NIR-I range) of the "A" pattern through a 5 mm thick tissue (Figure S13), compared to the sharp letter NIR-II image through a 9 mm thick tissue (Figure 4b). Moreover, the ability to resolve two NIR-II

DOI: 10.1021/jacs.6b08973
J. Am. Chem. Soc. 2016, 138, 16192−16195

line images with a threshold distance of 3 mm and two dot images with a distance of 4 mm through a 4 mm thick tissue suggests a lateral resolution ~3−4 mm at this imaging depth in biological tissues (Figure S14; organic phase particles were utilized). To demonstrate further the suitability of ICG-sensitized CSS nanocrystals for bioimaging, we employed an amphiphilic polymer DSPE-mPEG-2000 (1,2-distearoyl-*sn*-glycero-3-phosphoethanolamine-*N*-methoxy (polyethylene glycol)-2000) to encapsulate the ICG-sensitized Er doped CSS nanocrystals, thereby transferring them into the aqueous phase. Our hydrodynamic size measurement (over a period of 7 days), luminescence measurement (over 6 h), as well as HeLa cell viability test (dose of 0−1 mg/mL, 24 and 48 h) suggest that these aqueous forms are stable in vivo (but with a decreased luminescence intensity) and they exhibit negligible cytotoxicity (Figures S15−17). After subcutaneous injection of these aqueous suspended nanoparticles (0.2 mL of 2 mg/mL) into a mouse with a depth of ~3 mm, a clear NIR-II image of the injection point was obtained (Figure 4c).

In conclusion, we have described a hybrid organic−inorganic system consisting of epitaxial $NaYF_4$:Yb^{3+}/X^{3+}@$NaYbF_4$@$NaYF_4$:Nd^{3+} (X = null, Er, Ho, Tm, or Pr) CSS nanocrystals with ICG attached to the surface. The designated cascade energy transfer pathway: ICG → Nd^{3+} (outer shell) → Yb^{3+} (inner shell) →Yb^{3+}/X^{3+} (core) is able to yield a set of multiple narrow band emissions in the NIR-II range with a large Stokes-shift (>200 nm). The attachment of ICG not only enhances the brightness of these CSS nanocrystals by ~4-fold but also provides a broad excitation band of 700−860 nm. Moreover, NIR-II emissions from these ICG-sensitized CSS nanocrystals enable a clear observation of sharp image through chicken breast tissue with a depth of 9 mm, and signal detection at a depth of 23 mm. The achieved image is more contrast than that from Yb/Tm-codoped upconverting nanocrystals (excited at 980 nm, emission at 800 nm, in the NIR-I window), which are well-established for deep optical bioimaging. Subcutaneous injection of aqueous suspension of phospholipid-encapsulated ICG-sensitized CSS nanocrystals into a mouse additionally demonstrated their potential use for NIR-II bioimaging.

■ ASSOCIATED CONTENT

Supporting Information

The Supporting Information is available free of charge on the ACS Publications website at DOI: 10.1021/jacs.6b08973.

Additional experimental details (PDF)

■ AUTHOR INFORMATION

Corresponding Authors

*G.C. chenguanying@hit.edu.cn

*P.N.P. pnprasad@buffalo.edu

Notes

The authors declare no competing financial interest.

■ ACKNOWLEDGMENTS

This work was supported in part by the Air Force Office of Scientific Research (Grant No. FA9550-15-1-0358), the National Natural Science Foundation of China (51672061), and the Fundamental Research Funds for the Central Universities, China (AUGA5710052614 and AUGA8880100415). We acknowledge Nick Lechocinski from Axiom Optics for providing the WiDy InGaAs NIR CCD camera.

■ REFERENCES

(1) Chen, G.; Qiu, H.; Prasad, P. N.; Chen, X. *Chem. Rev.* **2014**, *114* (10), 5161−5214.

(2) Ntziachristos, V.; Ripoll, J.; Wang, L. H. V.; Weissleder, R. *Nat. Biotechnol.* **2005**, *23* (3), 313−320.

(3) Hilderbrand, S. A.; Weissleder, R. *Curr. Opin. Chem. Biol.* **2010**, *14* (1), 71−79.

(4) Prasad, P. N. *Introduction to Biophotonics*; John Wiley& Sons: Hoboken, NJ, 2003; p 633.

(5) Chen, G.; Shen, J.; Ohulchanskyy, T. Y.; Patel, N. J.; Kutikov, A.; Li, Z.; Song, J.; Pandey, R. K.; Ågren, H.; Prasad, P. N.; Han, G. *ACS Nano* **2012**, *6* (9), 8280−8287.

(6) Welsher, K.; Sherlock, S. P.; Dai, H. *Proc. Natl. Acad. Sci. U. S. A.* **2011**, *108* (22), 8943−8948.

(7) Bashkatov, A. N.; Genina, E. A.; Kochubey, V. I.; Tuchin, V. V. *J. Phys. D: Appl. Phys.* **2005**, *38* (15), 2543−2555.

(8) Antaris, A. L.; Chen, H.; Cheng, K.; Sun, Y.; Hong, G.; Qu, C.; Diao, S.; Deng, Z.; Hu, X.; Zhang, B.; Zhang, X.; Yaghi, O. K.; Alamparambil, Z. R.; Hong, X.; Cheng, Z.; Dai, H. *Nat. Mater.* **2016**, *15* (2), 235−242.

(9) Smith, A. M.; Mancini, M. C.; Nie, S. *Nat. Nanotechnol.* **2009**, *4* (11), 710−711.

(10) Hemmer, E.; Benayas, A.; Légaré, F.; Vetrone, F. *Nanoscale Horizons* **2016**, *1* (3), 168−184.

(11) Diao, S.; Blackburn, J. L.; Hong, G.; Antaris, A. L.; Chang, J.; Wu, J. Z.; Zhang, B.; Cheng, K.; Kuo, C. J.; Dai, H. *Angew. Chem.* **2015**, *127* (49), 14971−14975.

(12) Hong, G.; Diao, S.; Chang, J.; Antaris, A. L.; Chen, C.; Zhang, B.; Zhao, S.; Atochin, D. N.; Huang, P. L.; Andreasson, K. I.; Kuo, C. J.; Dai, H. *Nat. Photonics* **2014**, *8* (9), 723−730.

(13) Hong, G.; Lee, J. C.; Robinson, J. T.; Raaz, U.; Xie, L.; Huang, N. F.; Cooke, J. P.; Dai, H. *Nat. Med.* **2012**, *18* (12), 1841−1846.

(14) Hong, G.; Robinson, J. T.; Zhang, Y.; Diao, S.; Antaris, A. L.; Wang, Q.; Dai, H. *Angew. Chem.* **2012**, *124* (39), 9956−9959.

(15) Zhang, Y.; Hong, G.; Zhang, Y.; Chen, G.; Li, F.; Dai, H.; Wang, Q. *ACS Nano* **2012**, *6* (5), 3695−3702.

(16) Liu, Q.; Sun, Y.; Yang, T.; Feng, W.; Li, C.; Li, F. *J. Am. Chem. Soc.* **2011**, *133* (43), 17122−17125.

(17) Liu, J.; Liu, Y.; Bu, W.; Bu, J.; Sun, Y.; Du, J.; Shi, J. *J. Am. Chem. Soc.* **2014**, *136* (27), 9701−9709.

(18) Naczynski, D. J.; Tan, M. C.; Zevon, M.; Wall, B.; Kohl, J.; Kulesa, A.; Chen, S.; Roth, C. M.; Riman, R. E.; Moghe, P. V. *Nat. Commun.* **2013**, *4*, 2199.

(19) Kamimura, M.; Kanayama, N.; Tokuzen, K.; Soga, K.; Nagasaki, Y. *Nanoscale* **2011**, *3* (9), 3705−3713.

(20) White, K. A.; Chengelis, D. A.; Gogick, K. A.; Stehman, J.; Rosi, N. L.; Petoud, S. *J. Am. Chem. Soc.* **2009**, *131* (50), 18069−18071.

(21) Wang, Y.-F.; Liu, G.-Y.; Sun, L.-D.; Xiao, J.-W.; Zhou, J.-C.; Yan, C.-H. *ACS Nano* **2013**, *7* (8), 7200−7206.

(22) Chen, G.; Ohulchanskyy, T. Y.; Liu, S.; Law, W.-C.; Wu, F.; Swihart, M. T.; Ågren, H.; Prasad, P. N. *ACS Nano* **2012**, *6* (4), 2969−2977.

(23) Wang, R.; Li, X.; Zhou, L.; Zhang, F. *Angew. Chem., Int. Ed.* **2014**, *53* (45), 12086−12090.

(24) Xie, X.; Gao, N.; Deng, R.; Sun, Q.; Xu, Q.-H.; Liu, X. *J. Am. Chem. Soc.* **2013**, *135* (34), 12608−12611.

(25) Wen, H.; Zhu, H.; Chen, X.; Hung, T.; Wang, B.; Zhu, G.; Yu, S.; Wang, F. *Angew. Chem., Int. Ed.* **2013**, *52* (50), 13419−13423.

(26) Chen, G.; Damasco, J.; Qiu, H.; Shao, W.; Ohulchanskyy, T. Y.; Valiev, R. R.; Wu, X.; Han, G.; Wang, Y.; Yang, C.; Ågren, H.; Prasad, P. N. *Nano Lett.* **2015**, *15* (11), 7400−7407.

(27) Kraft, J. C.; Ho, R. J. Y. *Biochemistry* **2014**, *53* (8), 1275−1283.

(28) Li, Z. Q.; Zhang, Y. *Nanotechnology* **2008**, *19*, 345606.

(29) Dieke, G. H.; Crosswhite, H. M. *Appl. Opt.* **1963**, *2* (7), 675.

DOI: 10.1021/jacs.6b08973
J. Am. Chem. Soc. 2016, 138, 16192−16195